Journal of Materials Science: Materials in Electronics (2019) 30:8457–8470
https://doi.org/10.1007/s10854-019-01166-7

Strontium-substituted $La_{0.75}Ba_{0.25-x}Sr_xFeO_3$ (x = 0.05, 0.10 and 0.15) perovskite: dielectric and electrical studies

F. B. Abdallah[1] · A. Benali[1,2] · S. Azizi[1,3] · M. Triki[1] · E. Dhahri[1] · M. P. F. Graça[2] · M. A. Valente[2]

Received: 26 January 2019 / Accepted: 16 March 2019 / Published online: 20 March 2019
© Springer Science+Business Media, LLC, part of Springer Nature 2019, corrected publication 2019

Abstract
$La_{0.75}Ba_{0.25-x}Sr_xFeO_3$ perovskite compounds with different strontium concentrations were synthesized via the sol–gel method. X-ray diffraction (XRD) data indicated that all obtained samples crystallize in the orthorhombic structure with the Pnma space group. The dielectric properties of these samples, using complex impedance spectroscopy technique have been carried out as function of frequency and temperature as well. An adequate electrical equivalent circuit has been used to evaluate the grain and grain boundary contributions in complex impedance results. Furthermore, the AC conductivity spectra obey to Jonscher's universal power law. The behavior of the exponent "S" suggests that the conduction mechanism follows the overlapping large polaron tunneling (OLPT) process for x = 0.05, while for both compounds x = 0.10 and x = 0.15 the non-overlapping small polaron tunneling (NSPT) is the applicable model. The behavior of ε″ as a function of both frequency and temperature has been described by Giuntini model.

1 Introduction

During the last decades, rare earth orthoferrites have received special attention thanks to their vast range of technological applications [1]. In fact, they can be used as catalysts [2], fuel cells [3], oxygen permeation membranes and gas sensors [4, 5]. Lanthanum ferrite oxide, $LaFeO_3$, has been considered as one of the most important of the orthoferrite materials which exhibits a high stability over a wide range of temperatures [6].

Physical properties of $LaFeO_3$ are principally controlled by several factors. Among them doping is an effective way to improve their physical properties and to develop higher performances which are required for desired applications.

Our literature review shows that various reports are available on the study of the useful properties of $LaFeO_3$ by replacing La-site with alkaline metal such as Sr and Ba.

Recently, Cyza et al. [7] reported that the doping of $LaFeO_3$ with Sr leads to a decrease of grains size and on the surface which positively affects the physical properties such as sensitivity for the gases. On their part Yao et al. [8] synthesized $La_{1-x}Sr_x$ FeO_3 by sol–gel method. They found that as Sr content increases, the structural phase varies from orthorhombic to rhombohedral and cubic phase. They also investigated on the formaldehyde gas-sensing properties of Sr doped $LaFeO_3$. The experimental results show that the optimum operating temperatures of $La_{1-x}Sr_xFeO_3$ varies with Sr content. On the other hand Wang et al. [9] have done a detailed study of the Influence of Sr substitution on thermoelectric properties of $La_{1-x}Sr_xFeO_3$ ceramics. They found that the increase of Sr content reduces significantly both the electrical resistivity and the Seebeck coefficient, but slightly increases the high-temperature thermal conductivity. Adiabatic polaron hopping mechanism is found responsible for the conductivity in $La_{1-x}Sr_xFeO_3$, and the conductive carriers are thermally activated. Reactivity of $La_{1-x}Sr_xFeO_3$ perovskite oxides for chemical-looping reforming of methane was evaluated by He et al. [10]. They found that the substitution of La by Sr in $LaFeO_3$ would improve the amount of adsorbed oxygen of the perovskites, and inhibit methane decomposition in the methane reaction. Dielectric properties

✉ F. B. Abdallah
abdallahfatma72@gmail.com

[1] Laboratoire de Physique Appliquée, Faculté des Sciences, Université de Sfax, B.P. 1171, 3000 Sfax, Tunisia

[2] I3N and Physics Department, University of Aveiro, 3810-193 Aveiro, Portugal

[3] Equipe des Hydrures Métalliques, Laboratoire de Mécanique, Matériaux et Procédés, Ecole Nationale Supérieure d'Ingénieurs de Tunis (ENSIT, Ex ESSTT), Université de Tunis, 5 Avenue Taha Hussein, 1008 Tunis, Tunisia

of $La_{1-x}Sr_xFeO_3$ were also studied by Chern et al [11]. They observed that the activation energy decreases when the Sr-doping increases, with a strong dependence of temperature and frequency and high real dielectric constant.

On the other hand, the barium-doped lanthanum ferrite has also been the focus of intense studies. Sun et al. [12] reported a research on the structural and electrical properties of nanocrystalline $La_{1-x}Ba_xFeO_3$ for gas detection application. The results show that appropriate Ba-doping can restrain the growth of the grain size and improve the response of the $LaFeO_3$ based sensor to ethanol gas. Furthermore, the best response to ethanol gas was observed with Ba content equal to 0.25 mol. Based on solid-state reaction route, Masud et al. [13] prepared the $La_{0.5}Ba_{0.5}FeO_3$ system. They reported in detail the dielectric behavior of this system. Also, they observed that $La_{0.5}Ba_{0.5}FeO_3$ exhibit high dielectric permittivity. A complex impedance and modulus spectroscopic study shows two relaxation processes corresponding to grain and grain boundary contributions in this system. They demonstrated that magnetic field-dependent non-ferroelectric high dielectric behavior of $La_{0.5}Ba_{0.5}FeO_3$ might be important for its applications in devices. Zhang et al. [14] also investigated the physical properties of the same system. They observed interesting magnetic phase transition at low temperature under external pressure.

In our previous work [15], we have studied in detail the effects of strontium doping on the structural, morphological, optical and electrical properties of the $LaFeO_3$ doped barium, prepared according to the sol–gel method. The results obtained show that these properties have low strongly affected by the strontium content.

In present work, we are trying to investigate the effect of Sr-doping on the structural and dielectric properties of $La_{0.75}Ba_{0.25-x}Sr_xFeO_3$ nanocrystallines using impedance spectroscopy technique.

2 Experimental details

La $(NO_3)_3{\cdot}6H_2O$, Sr $(NO_3)_2$, Ba $(NO_3)_2$ and Fe $(NO_3)_3{\cdot}9H_2O$ of analytic purity were used as raw materials to prepare the $La_{0.75}Ba_{0.25-x}Sr_xFeO_3$ (x = 0.05, 0.10 and 0.15) ferrites by sol–gel method [16]. Firstly, all nitrates were separately dissolved in distilled water. Then citric acid and ethylene glycol were added to the solution under continuous stirring to get a homogeneous solution. This solution was heated until the gel formation. The obtained gel was dried and calcined at 300 °C for 12 h. At the end of the procedure, the resultant powders were pressed into pellets and heated at 900 °C for 24 h.

An X'Pert PRO MPD X-ray diffractometer with monochromator Cu-K_α radiation ($\lambda_{Cu} = 1.5405$ Å) was used to carry out the phase identification for the obtained samples. Complex impedance spectroscopy was used to study the electrical properties of our materials. This technique describes the electrical processes that occur in a system by applying an ac signal as input pressure [17]. It is used to analyze the phenomena of electrical conduction of materials and to separate the different contributions that could constitute this system (grain and grain boundary). The electrical measurements were carried out on pellet disks of about 8 mm in diameter and 1.3 mm in thickness in the temperature range from 250 to 310 K, in the frequency range from 100 Hz to 1 MHz, using an Agilent 4294 impedance analyzer.

3 Results and discussion

3.1 XRD studies

Figure 1a shows the XRD patterns of $La_{0.75}Ba_{0.25-x}Sr_xFeO_3$ (x = 0.05, 0.10 and 0.15) samples. A perovskite structure consisting of an orthorhombic phase was revealed by XRD patterns, in accordance with what previously reported [15]. The patterns show a slight shift in the most intense peak toward higher 2θ values with Sr content increasing, this indicates that the substitution of Sr has smaller ionic radii than the Ba. The shift of diffraction peaks toward higher angle reveals that the cell parameters of samples continuously decrease with the increase of Sr content. A typical Rietveld refinement analysis of x = 0.15 sample, using the FullProf software [18], is shown in Fig. 1b and their crystal structure is presented in Fig. 1c. The results of the refinement structural parameters of our samples are reported in Table 1. As clearly shown in this table, the bond lengths and bond angles show slight deviation when the doping increases.

3.2 Impedance studies

Impedance spectroscopy is a well-known as a powerful technique for investigation of the electrical properties of materials. Here, the real part of impedance (Z') as a function of frequency at several temperatures is shown in Fig. 2. The behavior of Z' observed in our samples shows three distinct regions in which changes are clearly visible with change in temperature and frequency. The first one (R-I) is at low frequency in which the values of Z' are frequencies independent and decrease with temperatures increasing. In the second one (R-II), the magnitude of Z' is found to decrease gradually with the rise of both frequency and temperature, due to the high mobility of charge carriers that indicates an increase

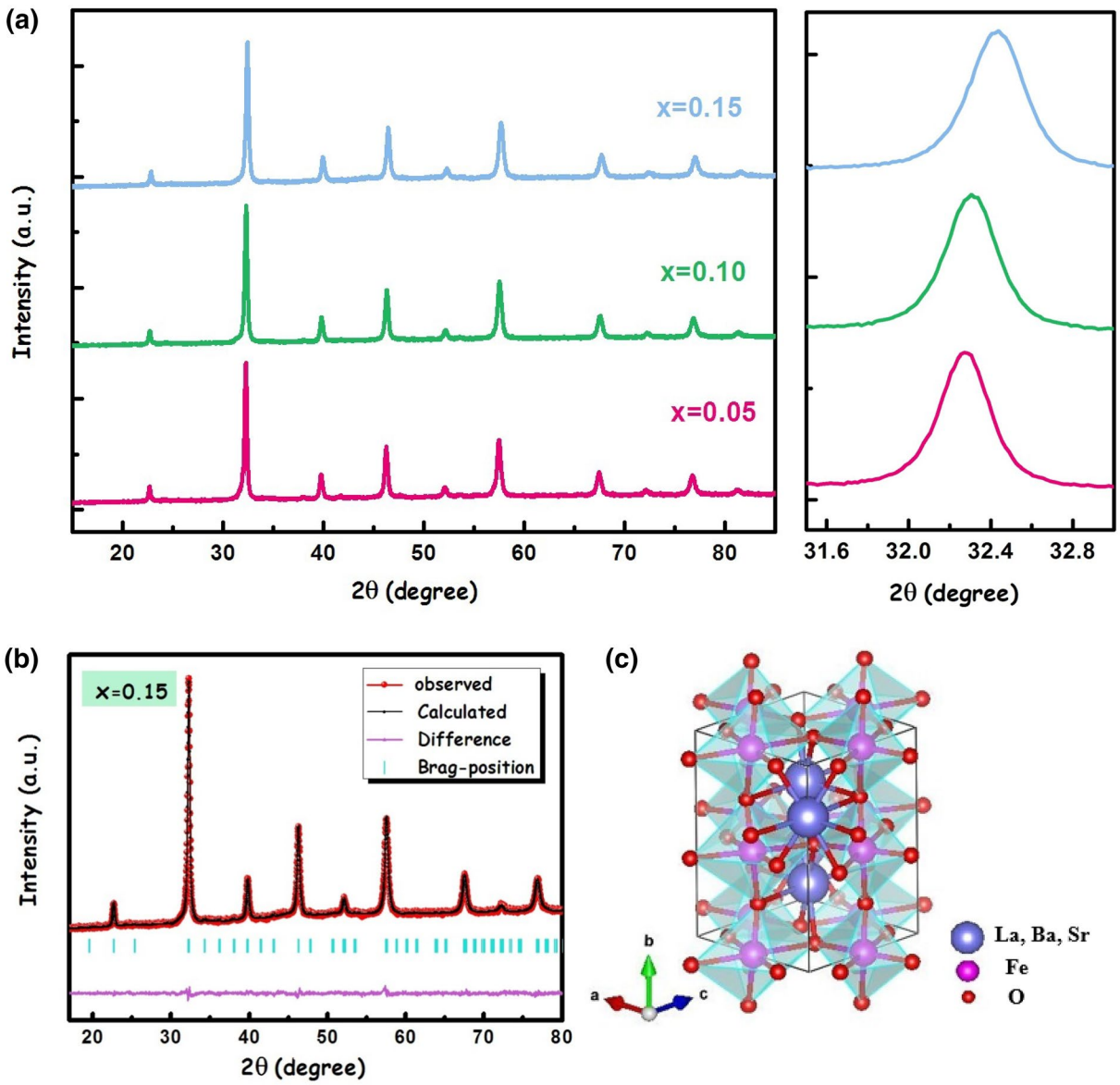

Fig. 1 XRD patterns for $La_{0.75}Ba_{0.25-x}Sr_xFeO_3$ (x = 0.05, 0.1 and 0.15) compounds (**a**) rietveld refinement plot for x = 0.15 sample (**b**) and crystal structure (**c**)

in AC conductivity with increasing both temperature and frequency. At higher frequencies (R-III), the Z' merges irrespective of temperature. This result may possibly be related to the release of space charge as a result of reduction of the barrier properties of the materials [16, 19].

The plots of the frequency dependence of imaginary part of impedance Z″ for all compounds is shown in Fig. 3. One can see that the Z″ values attains a peak maxima at a particular frequency (f_{max}) known as the relaxation frequency [20]. It is worth noting that the peaks are shifted to higher frequencies with increasing temperature. Such behavior indicates the presence of relaxation in our materials [21].

To provide the characteristic activation energy of the relaxation process, the plot of Ln(f_{max}) (relaxation frequencies corresponding to Z''_{max}) versus 1000/T is shown in Fig. 4. The temperature dependence of the relaxation frequency follows the Arrhenius law:

$$f_{\max} = f_0 \exp\left(-E_a / k_B T\right) \quad (1)$$

where f_0 is the pre-exponential factor, k_B is the Boltzmann constant and E_a is the activation energy for the relaxation. Using the slope of the fitted straight line, the activation energy values have been calculated and have been found

Table 1 Refined structural parameters for $La_{0.75}Ba_{0.25-x}Sr_xFeO_3$ (x = 0.05, 0.10 and 0.15) compounds

	x = 0.05	x = 0.10	x = 0.15
a (Å)	5.551 (8)	5.544 (6)	5.539 (7)
b (Å)	7.859 (4)	7.849 (4)	7.842 (5)
c (Å)	5.563 (8)	5.556 (6)	5.552 (7)
FeO (1)	1.9874 (8)	1.9746 (8)	1.9710 (80)
Fe–O (2)	1.44 (8)	2.395 (7)	2.374 (18)
Fe–O (2)	2.24 (7)	1.882 (3)	1.91 (2)
⟨Fe–O (2)⟩	1.889	2.083	2.085
⟨La(Ba, Sr)–O⟩	2.24	2.375	2.32
Fe–O(1)–Fe	162.69 (7)	167.24 (4)	168.26 (4)
Fe–O(2)–Fe	129 (3)	132.8 (5)	132.1 (8)
⟨Fe–O– Fe⟩	143.345	150.02	150.18

equal to 0.278, 0.283 and 0.306 eV for x = 0.05, 0.10 and 0.15, respectively. So, the substitution of barium atoms by the strontium ones leads to an increase of the activation energy.

Figure 5 shows Nyquist plots of $La_{0.75}Ba_{0.25-x}Sr_xFeO_3$ compounds. The impedance spectra are characterized by the appearance of semicircles where the diameter decreases with increasing temperature, referring to pronounced increase of DC conduction [22]. The impedance data are fitted using Z-view software [23] and the best fit are obtained when employing an equivalent circuit, as shown in Fig. 6, consisting of a series combination of grains boundary (R_{gb}–CPE_{gb}) and grains (R_g–C_g).

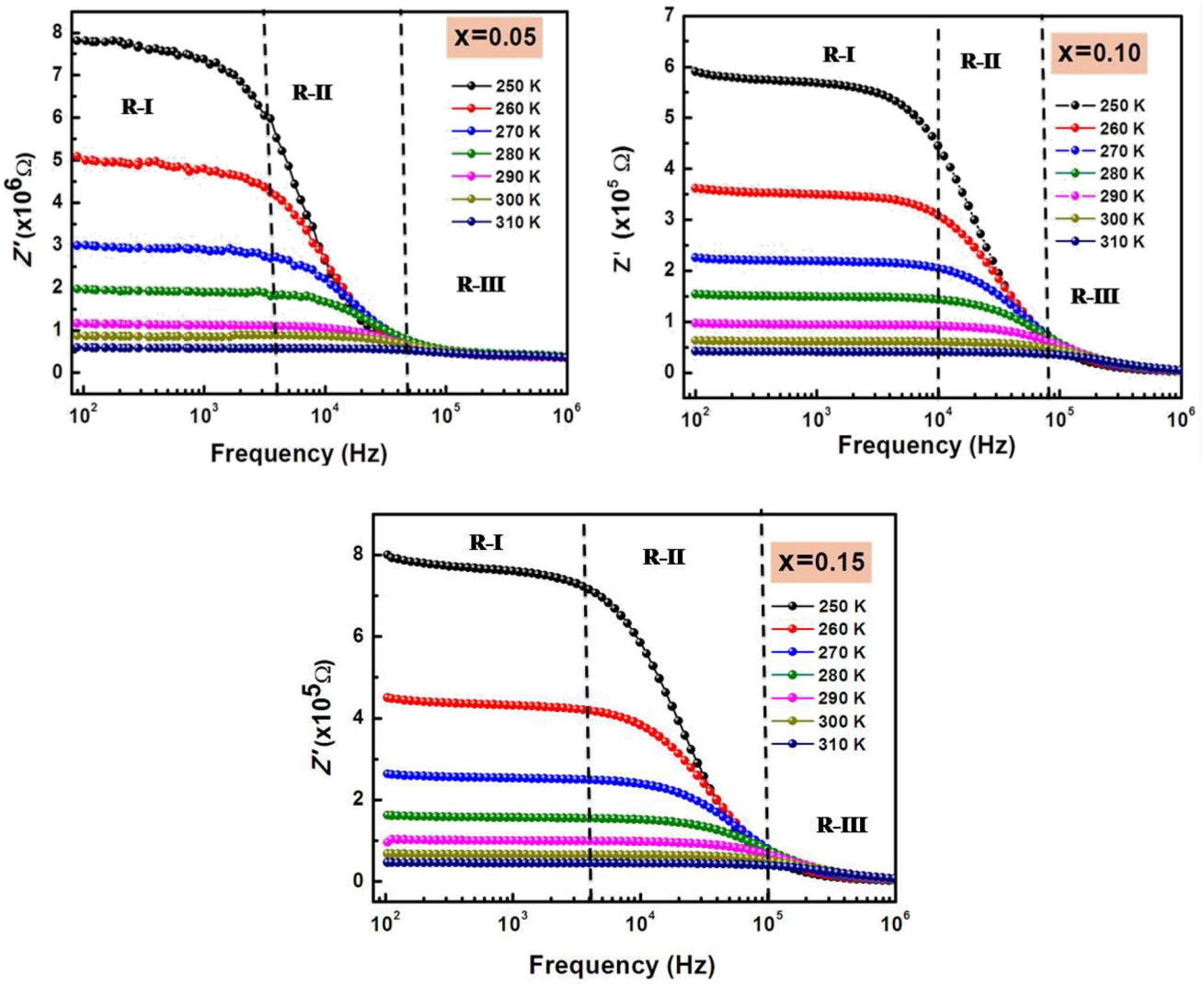

Fig. 2 The frequency dependence of the real (*Z*′) part of the complex electrical impedance at several measurement temperatures

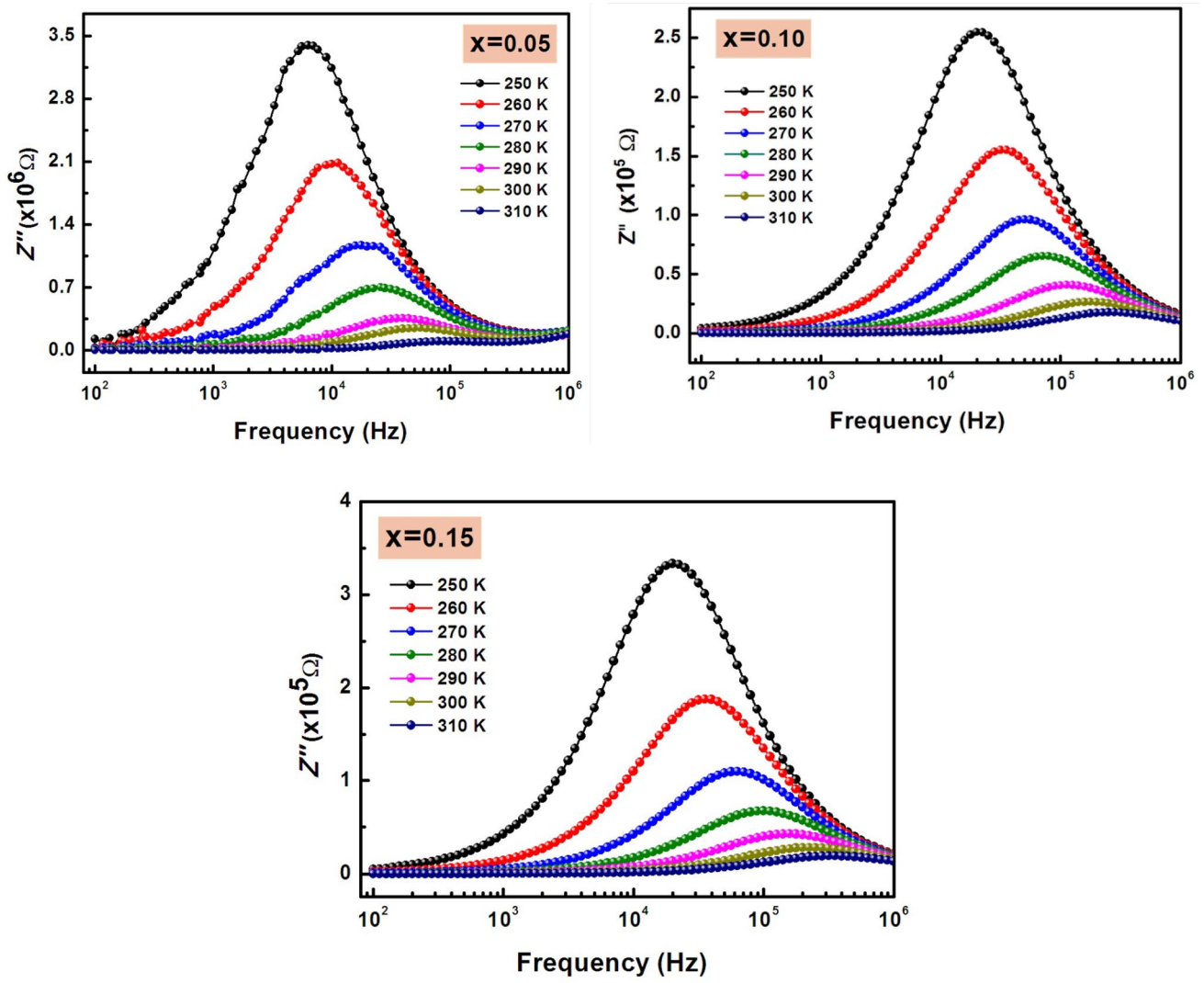

Fig. 3 The frequency dependence of the imaginary (Z″) part of the complex electrical impedance at several temperatures

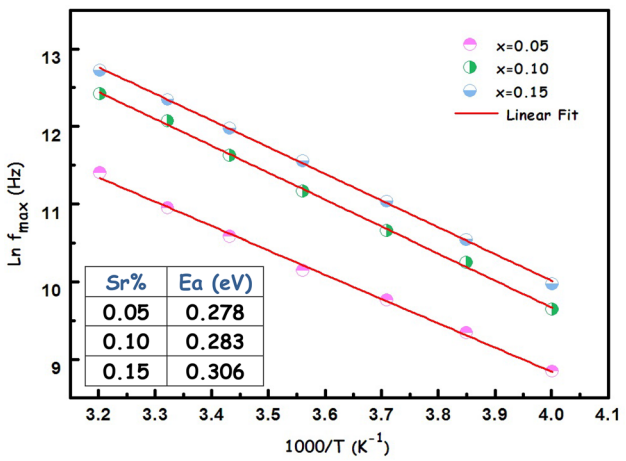

Fig. 4 The Arrhenius plots shows depedence f_{max} versus 1000/T. Inset figure is the activation energy E_a values

The constant phase element (CPE) impedance is given by the following relation:

$$Z_{CPE} = \frac{1}{Q(j\omega)^{\alpha}} \quad (2)$$

where Q is a proportional factor, ω is the angular frequency, and α is the parameter which estimates the deviation from the ideal capacitive behavior. α is zero for the pure resistive behavior and is the unit for the capacitive.

The values of all fitted parameters are presented in Table 2. We can see from this table that the grain boundary resistance values decrease with the increase of temperature, indicating a semi-conducting behavior for all samples [21]. Furthermore, it has been found that the values of R_{gb} are

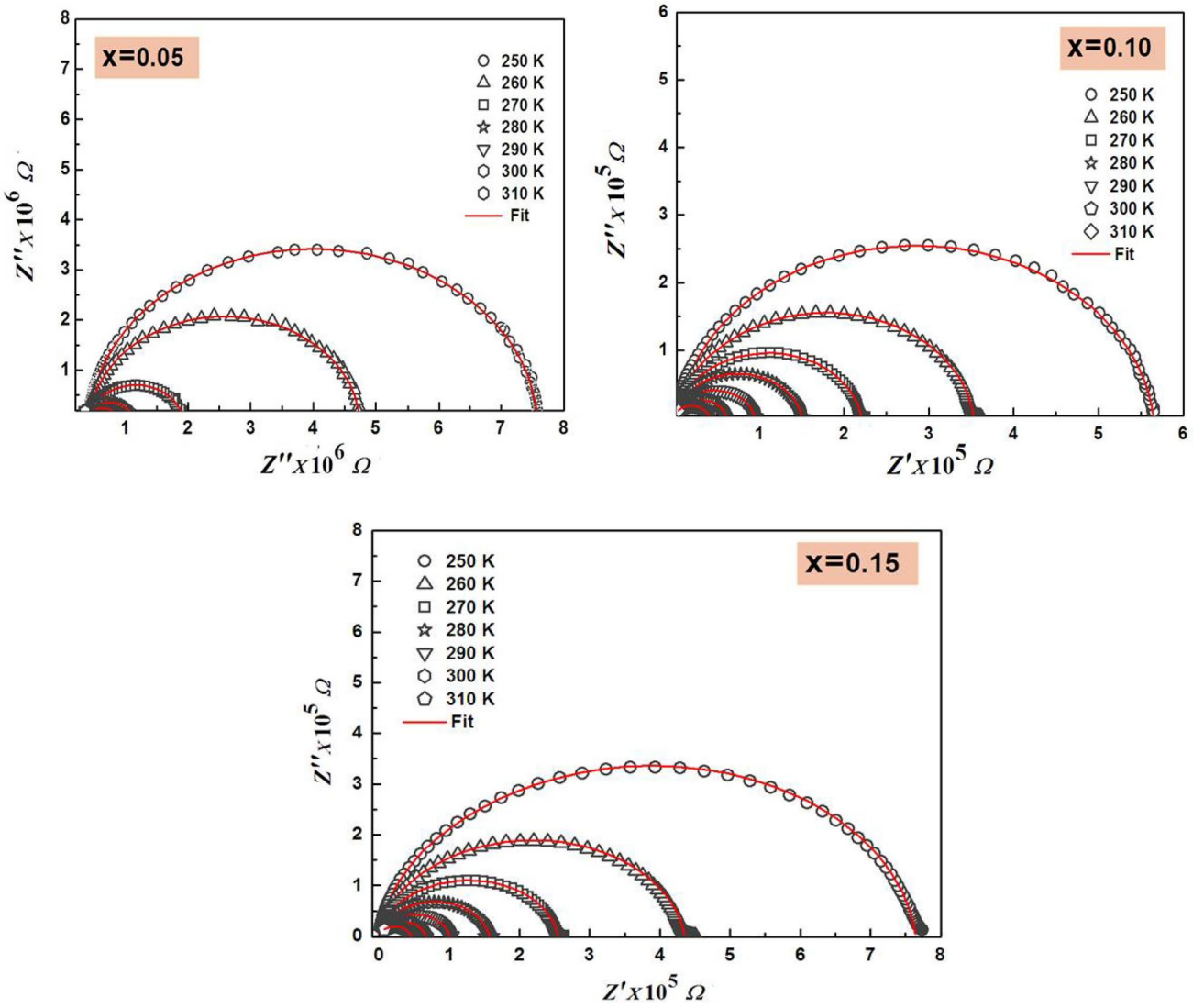

Fig. 5 Nyquist plot of impedance data at several temperatures

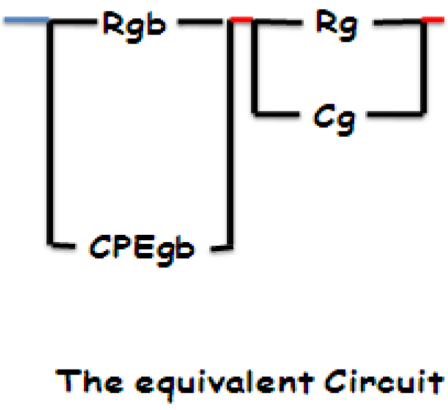

Fig. 6 The equivalent circuit for impedance

larger than those of R_g. This is assigned to the fact that the atomic arrangement near the grain boundary region is disordered, resulting in an increase of the electron scattering.

The logarithmic variation of the deduced R_{gb} and R_g with the inverse of temperature is shown in Fig. 7a and b. The activation energy can be obtained using the Arrhenius law:

$$R_{g,gb} = R_0 \exp\left(-E_a / k_B T\right) \tag{3}$$

where R_0 represents the pre-exponential constant or characteristic resistance, k_B is the Boltzmann constant, and E_a is the activation energy.

It is worth noticing from Fig. 7 that the activation energy values for grain boundaries are found to be slightly higher

Table 2 Parameters of equivalent circuits deduced from the complex diagram at several temperatures for $La_{0.75}Ba_{0.25-x}Sr_xFeO_3$ (x = 0.05, 0.10 and 0.15) compounds

	T (K)	250	260	270	280	290	300	310
x = 0.05	R_{gb} (× 10^5 Ω)	71.54	43.03	14.78	11.17	7.38	4.48	3.93
	CPE_{gb} (× 10^{-12}F)	4.66	4.70	6.565	7.62	8.27	4.17	0.041
	α	0.9709	0.973	0.965	0.969	0.9703	1.039	1.092
	R_g (× 10^5 Ω)	4.266	4.348	4.349	4.002	3.849	4.172	1.793
	C_g (× 10^{-13}F)	1.548	1.586	1.605	1.625	1.69	1.768	1.322
x = 0.10	R_{gb} (× 10^5 Ω)	5.598	2.183	2.145	1.179	0.9443	0.6134	0.4088
	CPE_{gb} (× 10^{-11}F)	2.779	3.767	3.188	4.763	5.151	5.326	5.132
	α	0.9564	0.9263	0.9244	0.9068	0.9045	0.9055	0.91
	R_g (× 10^3 Ω)	4.923	6.789	5.709	4.231	2.778	1.949	1.404
	C_g(×10^{-8}F)	9.451	9.131	9.05	8.161	7.61	7.136	6.7
x = 0.15	R_{gb} (×10^5Ω)	7.101	4.014	2.451	1.439	0.9604	0.627	0.3389
	CPE_{gb} (×10^{-11}F)	2.579	30.913	3.814	2.9	4.118	4.709	10.57
	α	0.9325	0. 915	0.9013	0.9216	0.9021	0.898	0.8604
	R_g (×10^4Ω)	5.498	3.444	1.042	1.005	0.3994	0.346	0.1133
	C_g (×10^{-10}F)	0.4704	0.616	2.218	4.897	2.358	1.18	2.182

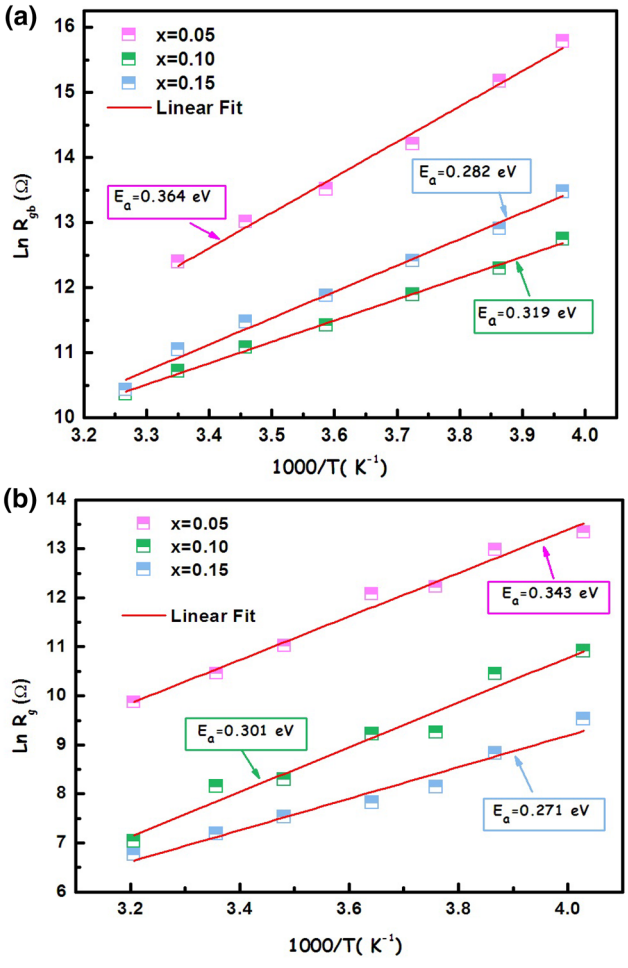

Fig. 7 The Arrhenius plots shows dependence resistances (**a**) grain boundary (R_{gb}) and (**b**) grain (R_g) versus 1000/T

than that of grains indicating higher resistive behavior than that of grains.

3.3 Conductivity studies

In order to understand the conduction behavior and to determine the parameters that may control the conduction processes in the $La_{0.75}Ba_{0.25-x}Sr_xFeO_3$ (x = 0.05, 0.10 and 0.15) samples, we plotted the variation of AC conductivity with frequency at operating temperatures from 250 to 310 K. As shown in Fig. 8, the conductivity increases with increasing frequency and temperature in all the samples. We notice that at low frequencies, the conductivity spectra are independent of the frequency for each temperature. For high frequencies values, these spectra are found to increase with frequency. According to Jonscher's power-law [24], the frequency dependence of the conductivity is expressed as:

$$\sigma(\omega) = \sigma_{dc} + A\omega^S \quad (4)$$

In this expression σ_{dc} is the direct current conductivity, A is a constant depending on temperature and the exponent "S" represents the degree of interaction between mobile ions and its surrounding lattices.

Experimental conductivity spectra are adjusted using the equation (Eq. 4). The fitting results are summarized in Table 3. The DC conductivity as a function of the inverse of the absolute temperature is shown in Fig. 9. This variation can be described by the Arrhenius equation as [25]:

$$\sigma_{dc} = \sigma_0 \exp\left(-E_a/k_B T\right) \quad (5)$$

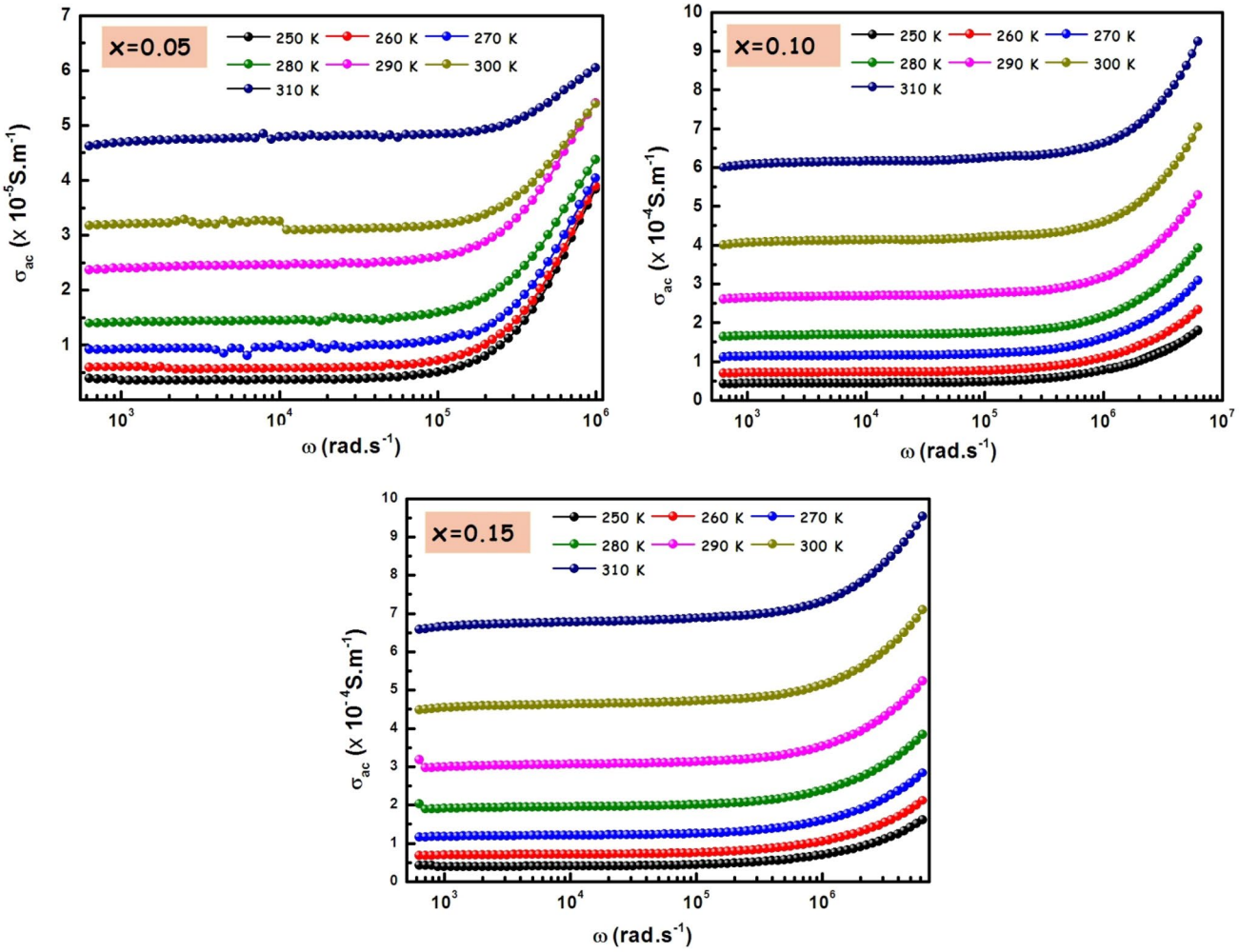

Fig. 8 Frequency dependency of conductivity for $La_{0.75}Ba_{0.25-x}Sr_xFeO_3$ (x = 0.05, 0.10 and 0.15) compounds

Table 3 The Jonscher's power-law fitting results of ac conductivity for $La_{0.75}Ba_{0.25-x}Sr_xFeO_3$ (x = 0.05, 0.10 and 0.15) compounds

	T(K)	250	260	270	280	290	300	310
x = 0.05	σ_{dc} (10^{-5} S m^{-1})	3.347	5.526	9.137	14.042	24.100	31.571	47.432
	A ($\times 10^{-12}$)	2.803	2.911	2.949	7.516	8.604	5.269	7.269
	S	1.094	0.987	0.901	0.866	0.823	0.838	0.902
x = 0.10	σ_{dc} (10^{-5} S m^{-1})	4.285	7.031	11.321	16.670	26.630	41.087	61.427
	A ($\times 10^{-10}$)	8.695	8.513	7.350	5.473	2.716	1.109	0.646
	S	0.745	0.776	0.799	0.833	0.888	0.948	0.987
x = 0.15	σ_{dc} (10^{-5} S m^{-1})	3.938	6.931	11.879	19.334	30.835	46.002	67.394
	A ($\times 10^{-10}$)	8.501	11.481	10.669	9.069	7.933	7.469	6.667
	S	0.758	0.761	0.770	0.788	0.811	0.843	0.87

where σ_0 is a pre-exponential factor and E_a is the activation energy. From the slopes of the linear fit, we can estimate the values of the activation energies associated with DC conduction. These values are found to be 0.289, 0.332 and 0.376 eV for x = 0.05, 0.10 and 0.15, respectively. The activation energy values obtained from both Arrhenius plots of σ_{dc} and the frequency corresponding to the peaks of the imaginary part of the impedance, in the same temperature

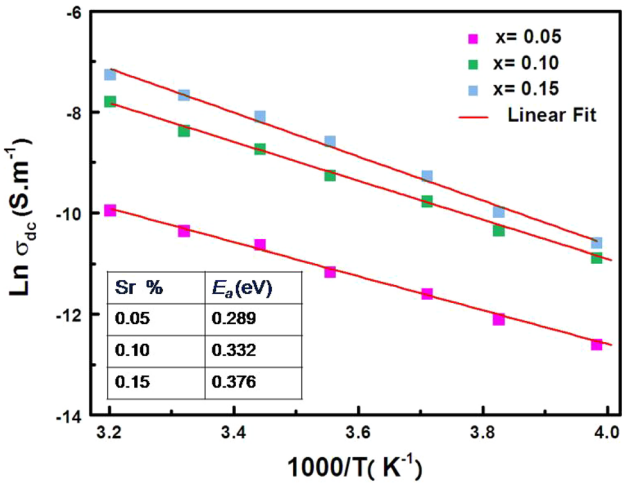

Fig. 9 Variation of the $\mathrm{Ln}(\sigma_{dc})$ as a function 1000/T for $La_{0.75}Ba_{0.25-x}Sr_xFeO_3$ (x = 0.05, 0.10 and 0.15) compounds. Inset figure is the activation energy E_a values

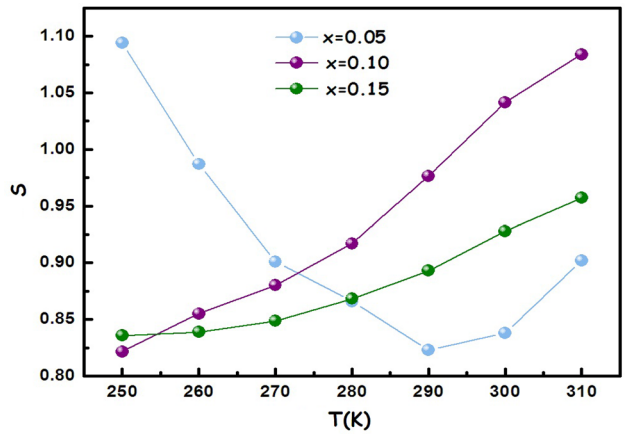

Fig. 10 Temperature dependence of the exponent **S** for $La_{0.75}Ba_{0.25-x}Sr_xFeO_3$ (x = 0.05, 0.10 and 0.15) compounds

range, are found to be close. The comparable values of activation energy increases with the increase of Sr doping. Thus, it can be assumed that the Sr content contributes indirectly in electrical conductivity.

The variation of the exponent "S" as a function of the temperature for all the compounds is shown in Fig. 10. As we can notice for x = 0.05, that this parameter decreases with increase in temperature and attains a minimum value then further increases suggesting the conduction to be mediated by overlapping large polaron tunneling (OLPT) process [26]. While, for x = 0.10 and x = 0.15, "S" increases with temperature increasing, indicating that the non-overlapping small polaron tunneling (NSPT) model is applicable for the both samples [27].

- The OLPT model (x = 0.05):

The overlapping large polaron tunneling (OLPT) model proposed by Long [28] where the exponent "S" depends on both temperature and frequency. According to this model, the large polaron wells at two sites overlap there by reducing the polaron hopping energy as follows [29, 30]:

$$W_H = W_{HO}\left(1 - r_p/R\right) \tag{6}$$

where r_p is the large polaron radius, R is the polaron intersite separation and W_{HO} is given by:

$$W_{HO} = e^2/4\varepsilon_p r_p \tag{7}$$

where ε_p is the effective dielectric constant. Assuming W_{HO} is constant for all sites, whereas the intersite separation R is a random variable.

The AC conductivity in overlapping large polaron tunneling conduction mechanism is [31]:

$$\sigma_{AC}(\omega) = \frac{\pi^4}{12} e^2 \left(k_B T\right)^2 \left[N\left(E_F\right)\right]^2 \frac{\omega R_\omega^4}{2\alpha k_B T + \left(W_{HO} r_P / R_\omega^2\right)} \tag{8}$$

In this expression, k_B is the Boltzmann constant, N is the density of states at the Fermi level, α the spatial extent of the polaron, and R_ω is the tunneling distance.

R_ω can be calculated by the quadratic equation:

$$R'^2_\omega + \left[W_{HO}\beta + \mathrm{Ln}\left(\omega\tau_0\right)\right]R' - W_{HO} r'_P \beta = 0 \tag{9}$$

where

$$R'_\omega = 2\alpha R_\omega, \quad \beta = \frac{1}{k_B T}, \quad r'_p = 2\alpha r_p$$

The frequency exponent S in OLPT model can be evaluated as [26]:

$$S = 1 - \frac{8\alpha R_\omega + \frac{6 W_{HO} r_p}{R_\omega k_B T}}{\left(2\alpha R_\omega + \frac{W_{HO} r_p}{R_\omega k_B T}\right)^2} \tag{10}$$

Table 4 Parameters used to OLPT model fitting for $La_{0.75}Ba_{0.25-x}Sr_xFeO_3$ (x = 0.05) compound at various frequencies

Frequencies (kHz)	$N(E_F)$ (10^{34} eV^{-1} m^{-1})	α (Å^{-1})	W_{HO} (eV)	r_p (Å^{-1})
500	13.144	4.412	0.308	2.996
700	9.539	3.246	0.366	2.404
1000	9.107	3.308	0.199	1.980

Parameters $N(E_F)$, α, W_{HO} and r_p for $La_{0.75}Ba_{0.20}Sr_{0.05}FeO_3$ obtained from fitting of experimental data are given in Table 4. It can be observed that $N(E_F)$ and r_p increase with frequency. In fact, the increase in the frequency stimulates the mobility of free charge which may cause the increment of the radius of the polaron and thus justifying the elevation of the AC conductivity with frequency.

- The NSPT model (x = 0.10 and x = 0.15):

According to the NSPT model, the exponent S is given by [32]:

$$S = 1 + \frac{4k_B T}{W_m - k_B T \mathrm{Ln}(\omega\tau_0)} \tag{11}$$

A first approximation of this equation, it reduces to the simple expression for the exponent S as:

$$S = 1 + \frac{4k_B T}{W_m} \tag{12}$$

The values of W_m (the bonding energy of the carrier in its localized sites) are determined from the Eq. 12 using the slope of the S (T) curves. The values are obtained in the order of 0.108 eV and 0.156 eV for x = 0.10 and 0.15 respectively. According to this model, the AC conductivity can be described by the following expression [33]:

$$\sigma_{AC} = \frac{(\pi e)^2 k_B T \alpha^{-1} \omega \left[N(E_F)\right]^2 R_W^2}{12} \tag{13}$$

Whither R_w is the tunneling distance is given by:

$$R_w = \frac{1}{2\alpha}\left[\mathrm{Ln}\left(\frac{1}{\omega\tau_0}\right) - \frac{W_H}{k_B T}\right] \tag{14}$$

Table 5 Parameters used to NSPT model fitting for $La_{0.75}Ba_{0.25-x}Sr_xFeO_3$ (x = 0.10 and 0.15) compounds at various frequencies

	500 kHz	750 kHz	1 MHz
x = 0.10			
$N(E_F)$ (10^{38} eV^{-1} m^{-1})	1.8743	9.833	73.540
α ($Å^{-1}$)	1.12	1.52	1.79
W_H (eV)	0.287	0.221	0.171
x = 0.15			
$N(E_F)$ (10^{39} eV^{-1} m^{-1})	0.855	4.309	13.346
α ($Å^{-1}$)	1.49	1.66	1.82
W_H (eV)	0.353	0.247	0.115

In Eqs. (13) and (14), the term α^{-1} is the spatial extension of the polaron, $N(E_F)$ represents the density of states near the Fermi level and W_H is the polaron hopping energy.

The $N(E_F)$, α and W_H were adjusted to fit the calculated curves of $\mathrm{Ln}(\sigma_{ac})$ versus T on the experimental curves. The obtained parameters are summarized in Table 5. As seen clearly that the both values of $N(E_F)$ and α increases with frequency, which is in accord with the literature [34]. Furthermore, the $N(E_F)$ values are reasonably high which suggests that the jump between site pairs dominates the charge transport mechanism in $La_{0.75}Ba_{0.25-x}Sr_xFeO_3$ samples [35].

3.4 Dielectric studies

The complex dielectric function is expressed as:

$$\varepsilon^* = \varepsilon' + j\varepsilon'' \tag{15}$$

where ε′ and ε″ are the real and imaginary parts of the complex permittivity. At selected temperature, we have plotted in Fig. 11 the frequency dependence of the imaginary part ε″ of the complex permittivity for x = 0.05, 0.10 and 0.15. From this plot it is clear that ε″ decreases rapidly with increase in frequency in the lower frequency region and become very stable at high frequency region. In the low frequency region, the values of the imaginary part of dielectric constant are very high. Indeed, the exchange of electrons between the Fe^{2+} and Fe^{3+} species serves to increase the orientation of dipoles and to the accumulation of charges at the interface between the grain and grain boundaries, which birth to all types of polarization such as electrodes, atomic and ionic [36]. On the other hand, at high frequency region, the exchange between the Fe^{2+} to Fe^{3+} species do not follow the alternating applied electric field; this leads the dielectric constant to remain constant across the measured temperature range [37].

The behavior of ε″ as a function of both frequency and temperature can be analyzed according to Giuntini et al [38]:

$$\varepsilon''(\omega) = (\varepsilon_0 - \varepsilon_\infty) 2\pi^2 N (ne/\varepsilon_0)^3 K T \tau_0^m W_M^{-4} \omega^m = B\omega^m \tag{16}$$

In this equations ε_0 is the static dielectric constant, ε_∞ the dielectric constant at "infinitely high" frequencies, N is the concentration of the localized sites, n is the number of charge carriers and W_M is the maximum barrier.

Figure 12 illustrated the variation of $\mathrm{Ln}(\varepsilon'')$ versus $\mathrm{Ln}(\omega)$ at different temperatures for all samples. These curves exhibit a series of straight lines with different slopes. From these slopes, the power "m" can be evaluated for different temperatures.

The variation of the power m (T) is plotted in the inset of Fig. 12. As clearly indicated in the insert, for x = 0.05, the values of m decreases with increasing temperature and reaches a minimum value then increases slightly with increasing

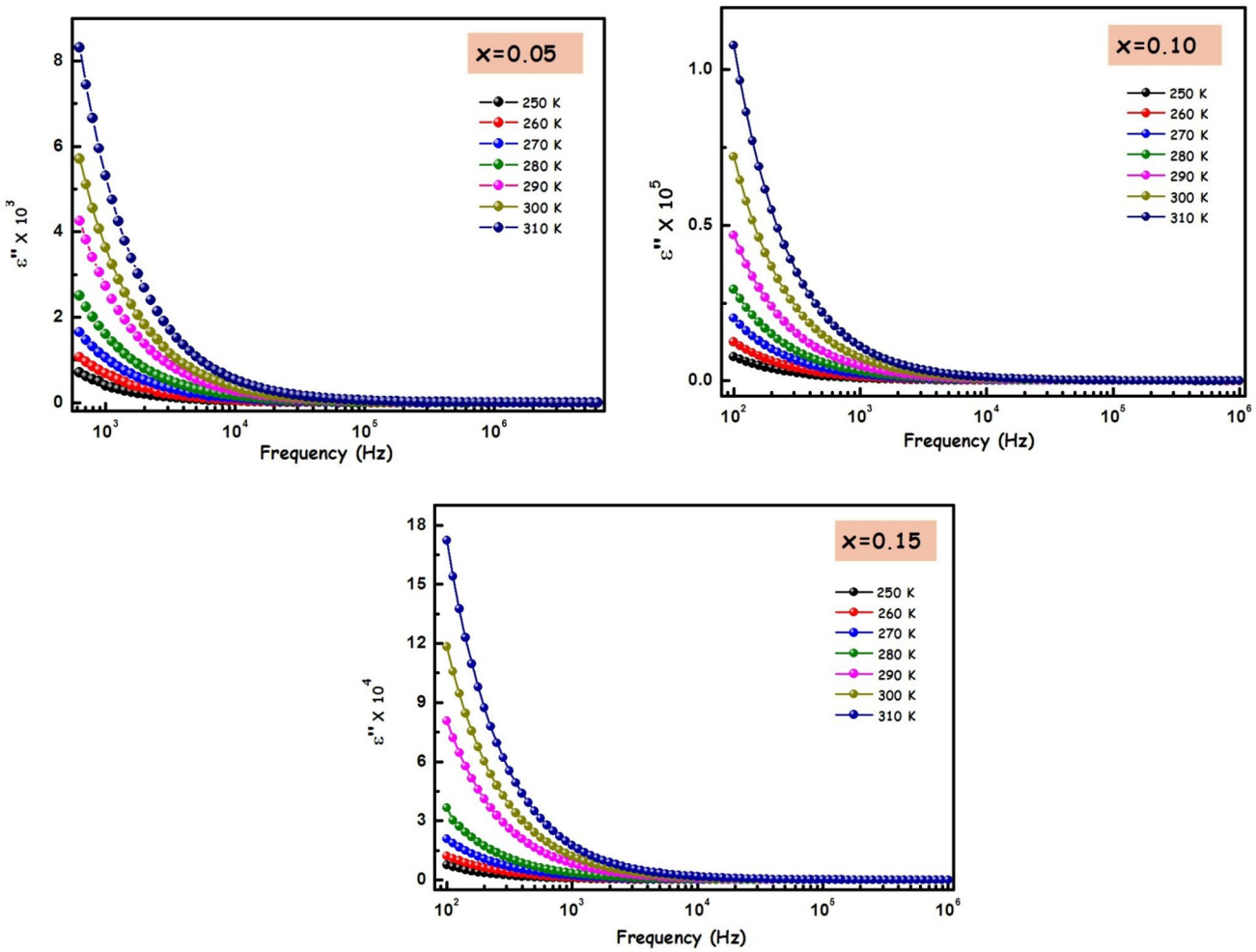

Fig. 11 Variation of ε″ with frequency at several temperatures for $La_{0.75}Ba_{0.25-x}Sr_xFeO_3$ (x = 0.05, 0.10 and 0.15) compounds

temperature which suggests the OLPT model [39]. An increase in m with the increase in temperature for both compounds x = 0.10 and 0.15 indicates the NSPT model [40]. It is obvious that both exponent "S" and exponent "m" have the same behavior trend. In fact, this result is satisfying the empirical law and confirms the correlation between ac conduction and the dielectric properties of semiconductor materials [41, 42].

3.5 Electrical modulus studies

The complex electric modulus formalism is necessary for the insight of the dielectric properties of the prepared samples. In Fig. 13 the plot of imaginary part of the electric modulus M″ at different temperatures is shown. It's worthy to note that the M″ curve exhibits a maximum at a characteristic frequency, which is known as the relaxation frequency (f_r). This maximum was shifted toward higher frequency side with increasing temperature. This behavior suggests that the dielectric relaxation is activated thermally and that a hopping process of charge carriers dominates intrinsically in grains [43].

Figure 14 displays the variation of the relaxation frequency with inverse of the temperature. It is noted that this variation exhibits an activated behavior follows the Arrhenius relation [44]:

$$f_r = f_0 \exp\left(-E_a / k_B T\right) \quad (17)$$

where E_a is the activation energy for relaxation and k_B is Boltzmann constant.

The activation energy values obtained from the fitting of curves are 0.303, 0.361 and 0.404 eV for x = 0.05, 0.1 and 0.15, respectively. It is observed that these values increase with the Sr-doping and that are in good agreement with those determined from the dc conduction.

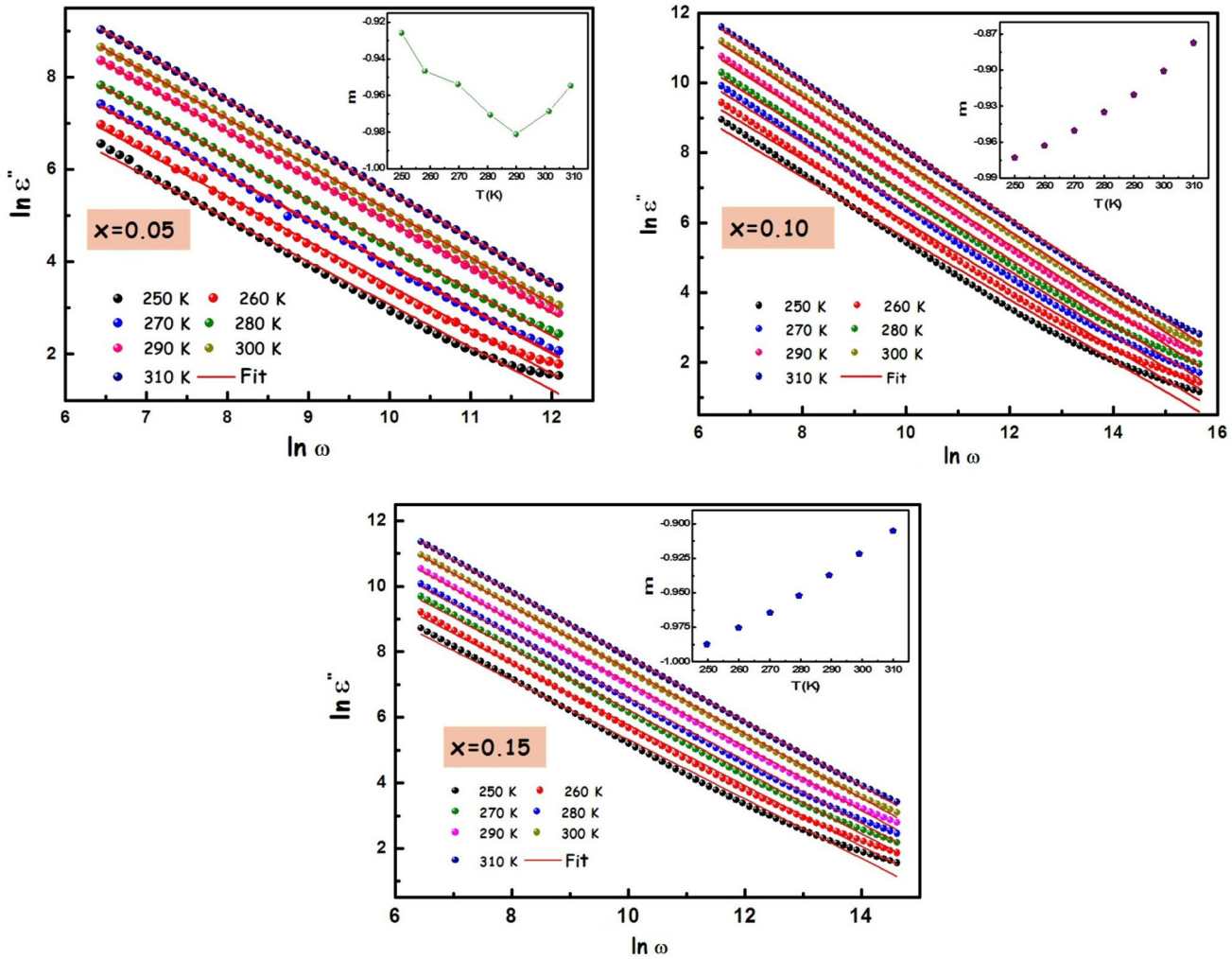

Fig. 12 Variation of ln(ε″) with ln(ω) at several temperature for $La_{0.75}Ba_{0.25-x}Sr_xFeO_3$ (x = 0.05, 0.10 and 0.15) compounds

4 Conclusion

In summary, we have synthesized the $La_{0.75}Ba_{0.25-x}Sr_xFeO_3$ perovskite with x = 0.05, 0.10 and 0.15 by sol–gel method. The impedance spectra are characterized by the appearance of semicircular arcs, well modeled in terms of electrical equivalent circuit confirmed the contribution of the grain and grain boundary. The Jonscher's power law is well fitted to the ac conductivity data. From fitting parameter, the temperature dependence of the frequency exponent "S" showed that for x = 0.05 the conduction mechanism can be attributed to the overlapping large polaron tunneling (OLPT) model and to non-overlapping small polaron tunneling model (NSPT) for the x = 0.10 and 0.15. Activation energies are extracted from several analyses: complex impedance and modulus spectra and DC conductivity spectra dependence temperature using the Arrhenius behaviors. It was found that the activation energies increase when the Sr^{2+} is increased. From the permittivity analysis, according to Giuntini's equation, the behavior of ε″ as a function of both frequency and temperature is analyzed and the temperature dependence of "m" is correlated with the AC conductivity.

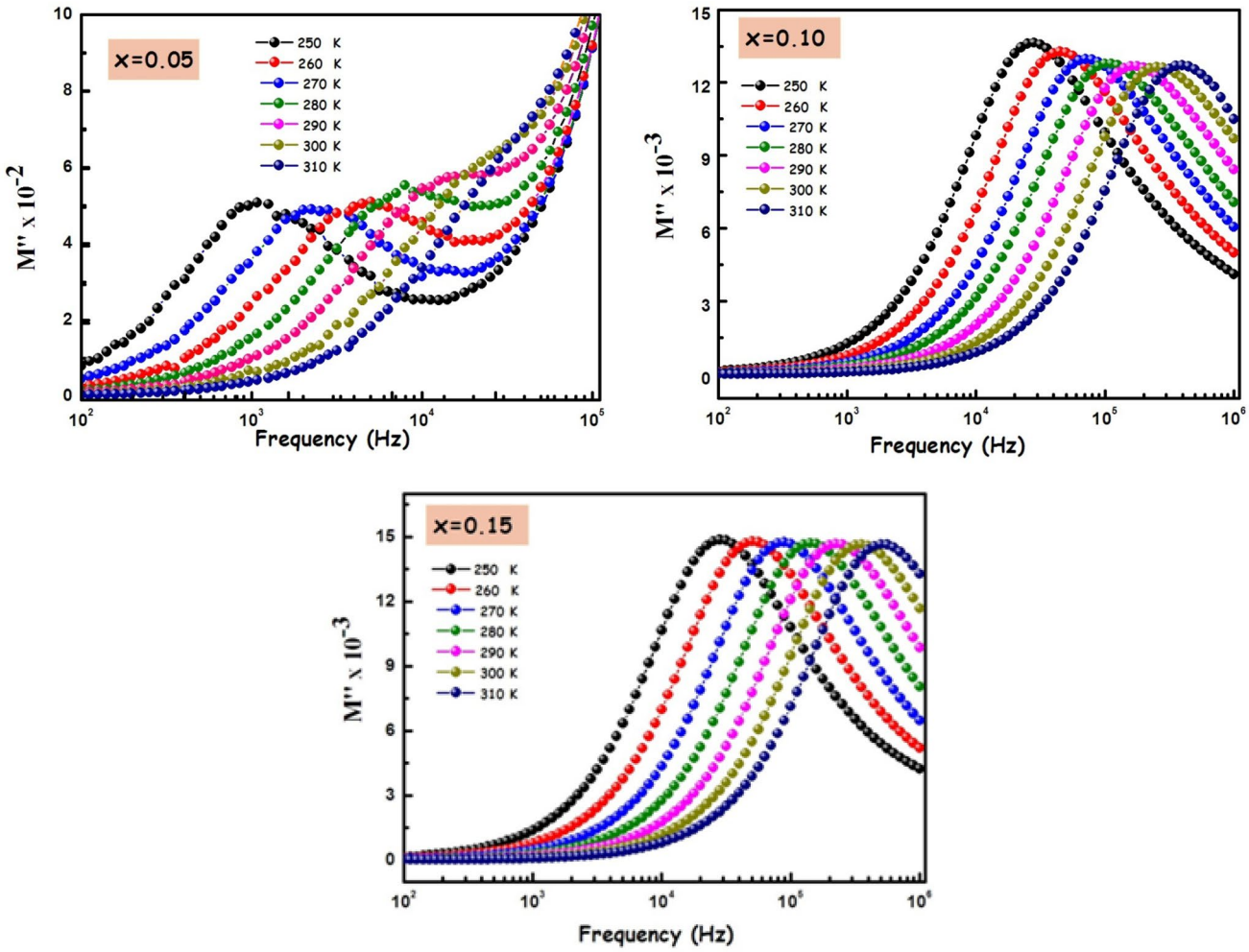

Fig. 13 Frequency dependence of imaginary part of the electric modulus M″ at several temperatures for $La_{0.75}Ba_{0.25-x}Sr_xFeO_3$ (x = 0.05, 0.10 and 0.15) compounds

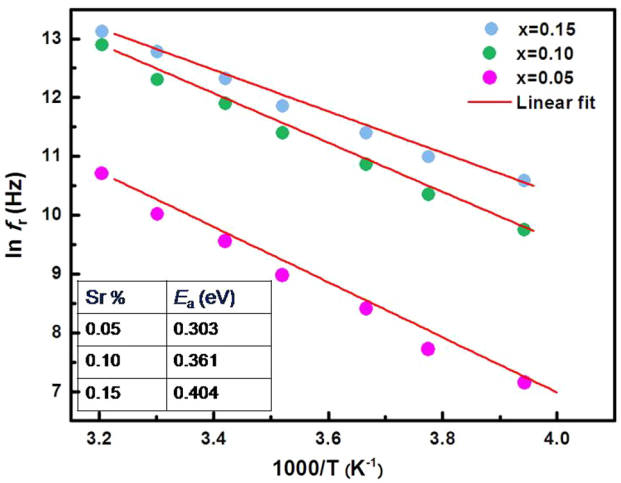

Fig. 14 Variation of the relaxation frequency with inverse of the temperature. Inset: the activation energy E_a values

References

1. M.C. Carotta, M.A. Butturi, G. Martinelli, Y. Sadaoka, P. Nunziante, E. Traversa, Sens. Actuators B **44**, 590–594 (1997)
2. Z.X. Wei, Y.Q. Xu, H.Y. Liu, C.W. Hu, J. Hazard. Mater. **165**, 1056–1061 (2009)
3. K. Huang, H.Y. Lee, J.B. Goodenough, J. Electrochem. Soc. **145**, 3220 (1999)
4. S.N. Tijare, M.V. Joshi, P.S. Padole, P.A. Mangrulkar, S.S. Rayalu, N.K. Labhsetwar, Int. J. Hydrog. Energy **37**, 10451–10456 (2012)
5. H. Xiao, C. Xue, P. Song, J. Li, Q. Wang, Appl. Surf. Sci. **337**, 65–71 (2015)
6. E.A. Tugova, V.F. Popova, I.A. Zvereva, V.V. Gusarov, Phys. Chem. **32**, 674–676 (2006)
7. A. Cyza, A. Kopia, Ł Cieniek, J. Kusinski, Mater. Today Proc. **3**, 2707–2712 (2016)
8. P.J. Yao, J. Wang, W.L. Chu, Y.W. Hao, J. Mater. Sci. **48**, 441–450 (2013)
9. H.C. Wang, C.L. Wang, J.L. Zhang, W.B. Su, J. Liu, M.L. Zhao, N. Yin, Y.G. Lv, L.M. Mei, Curr. Appl. Phys. **10**, 866–870 (2010)
10. F. He, X. Li, K. Zhao, Z. Huang, G. Wei, H. Li, Fuel **108**, 465–473 (2013)

11. G. Chern, W.K. Hsieh, M.F. Tai, K.S. Hsung, Phys. Rev. B **58**, 1252 (1998)
12. L. Sun, H. Qin, K. Wang, M. Zhao, J. Hu, Mater.Chem. Phys. **125**, 305–308 (2011)
13. G. Md, B.K. Masud, Chaudhuri, H.D. Yang, J. Phys. D Appl. Phys. **44**, 255403 (2011)
14. S. Zhang, S.L. Pi, Y. Zhang, J. Magn. Magn. Mater. **322**, 3381 (2010)
15. F.B. Abdallah, A. Benali, M. Triki, E. Dhahri, K. Nomenyo, G. Lerondel, J. Mater. Sci. Mater. Electron. **30**, 3349–3358 (2019)
16. F.B. Abdallah, A. Benali, M. Triki, E. Dhahri, M.P.F. Graca, M.A. Valente, Superlattices Microstruct. **117**, 260 (2018)
17. S. Lanfredi, A.C.M. Rodrigues, J. Appl. Phys. **86**, 4 (1999)
18. A. Benali, M. Bejar, E. Dhahri, M. Sajieddine, M.P.F. Graça, M.A. Valente, Mater. Chem. Phys. 149–150 (2015) 467–472
19. S. Brahma, R.N.P. Choudhary, A.K. Thakur, Phys. B **355**, 188–201 (2005)
20. H. Baaziz, N.K. Maaloul, A. Tozri, H. Rahmouni, S. Mizouri, K. Khirouni, E. Dhahri, Chem. Phys. Lett. **640**, 77–81 (2015)
21. A. Omri, M. Bejar, E. Dhahri, M. Es-Souni, M.A. Valente, M.P.F. Graça, L.C. Costa, J. Alloys Compd. **536**, 173 (2012)
22. A. Shukla, R.N.P. Choudhary, A.K. Thakur, J. Phys. Chem. Solids **70**, 1401 (2009)
23. D. Johnson, ZPlot, ZView Electrochemical Impedance Software, Version 2.3b (Scribner Associates, Inc., North Carolina, 2000)
24. A.K. Jonscher, *Universal Relaxation Law* (Chelsea Dielectric Press, London, 1996)
25. K.P. Padmasree, D.K. Kanchan, A.R. Kulkami, Solid State Ion. **177**, 475 (2006)
26. A. Ghosh, Phys. Rev. B **42**, 1388 (1990)
27. S. Mollah, K.K. Som, K. Bose, B.K. Chaudhuri, J. Appl. Phys. **74**, 931 (1993)
28. A.R. Long, Adv. Phys. **31**, 553 (1982)
29. I.G. Austin, N.F. Mott, Adv. Phys. **18**, 41 (1969)
30. D.K. Modak, U.K. Mandal, M. Sadhukhan, B.K. Chaudhuri, T. Komatsu, J. Mater. Sci. **36**, 2539–2545 (2001)
31. M. Tan, Y. Köseoğlu, F. Alan, E. Şentürk, J. Alloys Compd. **509**, 9399–9405 (2011)
32. S.R. Elliot, Adv. Phys. **36**, 135–217 (1987)
33. A. Benali, M. Bejar, E. Dhahri, M.F.P. Graça, L.C. Costa, J. Alloys Compd. **653**, 506 (2015)
34. S. Nasri, M. Megdiche, M. Gargouri, Ceram. Int. **42**, 943 (2016)
35. A.K. Roy, A. Singh, K. Kumari, K. Amar Nath, A. Prasad, K. Prasad, ISRN Ceram. (2012). https://doi.org/10.5402/2012/854831
36. N.K. Singh, P. Kumar, R. Rai, J. Alloys. Compd. **509**, 2957 (2011)
37. M. Idrees, M. Nadeem, M. Atif, M. Siddique, M. Mehmood, M.M. Hassan, Acta Mater. **59**, 1338 (2011)
38. J.C. Giuntini, J.V. Zanchetta, D. Jullien, R. Eholie, P.J. Houenou, J. Non-Cryst. Solids **45**, 57 (1981)
39. N. Weslati, I. Chaabane, A. Bulou, F. Hlel, Phys. B **441**, 42–46 (2014)
40. M. Ben Gzaiel, A. Oueslati, F. Hlel, M. Gargouri, Phys. E **83**, 405 (2016)
41. M.A.M. Seyam, Appl. Surf. Sci. **181**, 128–138 (2001)
42. S.R. Elliott, Phil. Mag. **36**, 1291 (1977)
43. K. Prabakar, S.A.K. Narayandass, D. Mangalaraj, Cryst. Res. Technol. **37**, 1094–1103 (2002)
44. P. Muralidharan, M. Venkateswarlu, N. Satyanarayana, J. Non-Cryst. Solids **351**, 583–594 (2005)

Publisher's Note Springer Nature remains neutral with regard to jurisdictional claims in published maps and institutional affiliations.